Journal of Controlled Release 368 (2024) 518–532

Contents lists available at ScienceDirect

Journal of Controlled Release

journal homepage: www.elsevier.com/locate/jconrel

Microenvironment-responsive smart hydrogels with antibacterial activity and immune regulation for accelerating chronic wound healing

Xiangtian Deng [a,b], Ye Wu [a], YunFeng Tang [a,b], Zilu Ge [a,b], Dong Wang [a,b], Cheng Zheng [c,*], Renliang Zhao [a,b,**], Wei Lin [d], Guanglin Wang [a,b]

[a] Department of Orthopedics, Orthopedics Research Institute, West China Hospital, Sichuan University, China
[b] Trauma medical center, Department of Orthopedics surgery, West China Hospital, Sichuan University, Chengdu 610041, China
[c] National Engineering Research Center for Biomaterials, Sichuan University, Chengdu, Sichuan 610041, China
[d] Department of Gynecology, West China Second Hospital, Sichuan University, Chengdu, China

ARTICLE INFO

Keywords:
Chronic wound healing
pH/ROS dual-responsiveness multifunctional dressing
Bacteria elimination
Macrophage polarization
Angiogenesis promotion

ABSTRACT

Current therapeutic strategies for chronic refractory wounds remain challenge owing to their unfavorable wound microenvironment and poor skin regeneration ability. Thus far, a regimen for effective chronic refractory wounds management involves bacterial elimination, alleviation of oxidative stress, inhibition of inflammatory response, and promotion of angiogenesis. In this work, an injectable glycopeptide hydrogel based on phenylboronic acid-grafted ϵ-polylysine (EPBA) and poly (vinyl alcohol) (PVA) with pH/reactive oxygen species (ROS) dual-responsive properties was prepared, which exerted intrinsic antibacterial and antioxidant properties. ROS-responsive micelles (MIC) loaded with herb-derived Astragaloside IV (AST) are introduced into the hydrogel before gelation. Attributed to the acidic condition and oxidative stress microenvironment of wound bed, the hydrogel gradually disintegrates, and the released EPBA could help to eliminate bacterial. Meanwhile, the subsequential release of AST could help to achieve anti-oxidation, anti-inflammatory, proangiogenic effects, and regulation of macrophage polarization to accelerate chronic wound healing. In addition, the wound repair mechanism of composite hydrogel accelerating skin regeneration was assessed by RNA-sequencing, exploring a range of potential targets and pathway for further study. Collectively, this multifunctional hydrogel dressing, matching different healing stages of tissue remodeling, holds a great potential for the treatment of chronic refractory wounds.

1. Introduction

Skin, as the human body's largest defensive organ, acts as the primary barrier to defend against external environmental hazards [1–3]. Owing to the accidental trauma, diabetes, immune-imbalance conditions, and other elements, the process of skin regeneration may be compromised, leading to chronic wounds following skin trauma [4]. Nowadays, managing chronic wounds is gradually emerging as a significant clinical dilemma to public health [5]. Within wound microenvironment, bacterial can proliferate significantly and cause wound infection [6]. Further, bacterial infections can contribute to chronic refractory wounds, an increase in wound area, permanent tissue damage, and even systemic infections [7,8]. During the repair progression of chronic refractory wounds, immune responses, especially through the modulation of macrophage polarization and phenotypes [9], play a virtual role in skin repairing and tissue regeneration. In response to wound microenvironment, macrophages could differentially polarize into pro-inflammatory macrophages (M1 type) and secrete significant amounts of pro-inflammatory cytokines in the early inflammatory stage [10]. M1 phenotype macrophages act an essential role in bacterial elimination and pathogen eradication when infection occurred. In contrary, M2 phenotype macrophages contribute to inhibiting inflammation and promoting skin regeneration and wound healing in the later stages of repairing [11,12]. Nevertheless, owing to the widespread proliferation of bacterial and heightened inflammation in chronic refractory wounds, macrophages have a tendency to polarize into the M1 phenotype. This result in the failure of the phenotypic transition from M1 to M2 type, causing an ongoing recruitment and activation of pro-

* Corresponding author.
** Corresponding author at: Department of Orthopedics, Orthopedics Research Institute, West China Hospital, Sichuan University, China.
E-mail address: zrldcd@163.com (R. Zhao).

https://doi.org/10.1016/j.jconrel.2024.03.002
Received 26 December 2023; Received in revised form 24 February 2024; Accepted 4 March 2024
Available online 12 March 2024

inflammatory cells, along with delayed wound healing [13,14]. Therefore, a promising wound dressing could prevent overactivation of M1 macrophages and promote macrophage polarization toward M2 to regulate immune response [15], thereby effective accelerating chronic wound healing.

Eliminating bacterial infection is an essential step for the promotion of chronic wound healing, which significantly improve the unfavorable conditions within the wound area. To eliminate bacterial infection, systemic or local administration of antibiotics are still the major antibacterial strategy owing to its advantages of outstanding sterilization ability. Nevertheless, owing to the abuse of antibiotics in the past few decades, multidrug-resistant superbugs have emerged and become a worldwide challenge for public health [16,17]. Antibacterial polypeptides such as ε-polylysine (EPL) have been extensively employed in chronic wounds owing to its superior biosafety (approved by FAD in USA) and wide-ranging antibacterial activity [18–20]. After eliminating bacterial infection and inhibiting inflammatory response, boosting angiogenesis could remarkably promote tissue repairing [21]. Astragaloside IV (AST), one of the primary active components extracted from Radix astragali, a classic Chinese herb medicine, is well regarded as a cardiovascular protector since it has various pharmacological performances, including antioxidative stress, suppressing inflammation, and promoting angiogenesis [22,23]. Also, increased studies confirmed that AST could accelerate wound healing through promoting macrophages polarize into M2 phenotypes [24]. Unfortunately, low water solubility, poor bioavailability, low penetration and rapid metabolism of AST hinders its clinical application in chronic wound treatment. Consequently, it is an urgent demand to prepare an intelligent material system which could efficiently improve drug solubility and bioavailability, achieve desired therapeutic effects, and promote tissue regeneration. Thus far, numerous biomaterials have been developed for treating hard-to-heal wounds, such as porous foams, lyophilized sponges, biocompatible membranes, nanofiber, and smart hydrogels [25,26]. Among these biomaterials, hydrogels are recognized as the most hopeful biomaterials for wound dressing owing to their three-dimensional porous networks, superior swelling capabilities, controllable physical properties, and good biocompatibility [27–29]. They can absorb wound exudates to maintain a moist condition, and have been utilized as a material system to encapsulate therapeutic agents to accelerate tissue remodeling [30,31]. Hence, the development of an intelligent hydrogel wound dressing possessing antibacterial, anti-inflammation, antioxidant, and angiogenesis ability holds significant importance for accelerating chronic wound healing.

Inspired by the above considerations, we have constructed a smart responsive multifunctional hydrogel dressing with injectability, inherent antibacterial properties, and pH/ROS dual-responsiveness. As illustrated in Scheme 1, phenylboronic acid (PBA)-grafted ε-polylysine (EPBA), and poly (vinyl alcohol) (PVA) solution were applied to construct the EPBA-PVA hydrogel through a dynamic phenylboronic acid−diol ester bonds. Following that, the AST-loaded micelles (MIC&AST) assembled from amphiphilic DSPE-thioketal-PEG (DSPE-TK-PEG) with a ROS responsive function were synthesized, which can achieve inflammation-induced AST release in the bacterial-infected wound microenvironment. Finally, MIC&AST was introduced to the EPBA-PVA hydrogel before gelation, and the EPBA-PVA@MIC&AST (EPMA) smart responsive multifunctional hydrogel with sequential drug release and pH/ROS dual-responsive properties was developed. Following the injection of hydrogel into the chronic wound site, the EPL in the composite hydrogel enable excellent broad-spectrum antibacterial ability. The secondary release of MIC&AST eradicated ROS and stimulate the polarization of macrophages toward the M2 phenotype, thus effectively ameliorating inflammation and accelerating skin regeneration in the proliferation phase. Meanwhile, the sustained release of AST from micelles could effectively promote angiogenesis and accelerate skin regeneration. Taken together, the intelligent EPMA hydrogel with cascading functional activities possessed great promise in the treatment of chronic refractory wounds.

2. Materials and methods

2.1. Materials

4-Formylphenylboronic acid, ϵ-polylysine (EPL) and sodium cyanoborohydride ($NaBH_3CN$) were obtained from Energy Chemical (Shanghai, China). Poly (vinyl alcohol) (PVA1788) were purchased from Haohong Scientific (Shanghai, China). Astragaloside IV (AST) was purchased from Yuanye Bio-Technology (Shanghai, China). DSPE-thioketal-PEG (DSPE-TK-PEG) was purchased from Ruixi Chemical (Xi'an, China).

2.2. Synthesis and characterization of EPBA

To prepare EPBA, 4.00 g of EPL was firstly weighed and dissolved in 80 mL of deionized water, then 2.65 g of 4-Formylphenylboronic acid was dissolved in 80 mL methanol and added to EPL solution under magnetic stirring. After reacted for 4 h in room temperature, 1.11 g of $NaBH_3CN$ was slowly added to the reaction mixture and reacted overnight. The crude product was then dialyzed (MWCO = 1.0 kDa) against deionized water for 5 days, and centrifuged (3000 rpm, 5 min) to obtain the EPBA solution. EPBA was obtained as white solid after lyophilization. The structure of EPBA was characterized by FTIR, ^{1}H NMR and UV spectra.

2.3. Synthesis and characterization of MIC&AST

The AST (mg) and DSPE-TK-PEG (mg) were dissolved in 1 mL of dimethyl sulfoxide, and the solution was added dropwise to deionized water under ultrasonic dispersion. The obtained solution was dialyzed (MWCO: 1000 kDa) against deionized water for 48 h and then filtrated through 0.45 μm filter to remove large aggregates, and the MIC&AST was prepared. The zeta potential and size distribution of MIC&AST were then evaluated by a Zetasizer (Malvern Zetasizer Nano ZS90). The mass of encapsulated AST was determined by HPLC.

2.4. Fabrication and of characterization of the EPBA-PVA and EPMA hydrogels

A PVA solution (10%, *w/v*) was obtained by dissolving the PVA solid to deionized water under 80 °C with magnetic stirring. EPBA solution (5%, w/v) was added to PVA solution with a ratio of 1:1 in volume to fabricate EPBA-PVA hydrogel. MIC&AST (AST 80 μM) was added to EPBA-PVA hydrogel to fabricate EPMA hydrogel. The morphologies of the EPBA-PVA and EPMA hydrogel were detected by SEM and EDS. The rheological properties, swelling ratio, degradation rate, adhesion property, pH/ROS-responsive abilities of the hydrogels were also evaluated. The details were presented in the Supporting Information.

2.5. Biocompatibility of the EPMA

The hemolysis test was conducted to detect the blood compatibility of the hydrogels. The cytocompatibility of the hydrogels was determined by using Human umbilical vein endothelial cells (HUVECs) and Mouse fibroblasts cells (3 T3-L1) cells. Blood compatibility of hydrogels was tested by hemolysis test. The biocompatibility of the hydrogels was determined by live/dead staining and cell counting kit-8 (CCK-8) kit. The details were presented in the Supporting Information.

2.6. Antioxidant efficiency and antibacterial property of the EPMA

The antioxidant property of the hydrogels was determined by two methods (DPPH free radical scavenging assay and reactive oxygen species assay). The antibacterial abilities of the EPMA were comprehensively evaluated by the optical density (OD) 600 method, standard plate

counting assay, and Live/Dead staining. The morphological changes of bacterial after different treatments were observed using SEM. Gram-positive *Staphylococcus aureus* (*S. aureus*) and gram-negative *Escherichia coli* (*E. coli*) were selected as models to detect the antibacterial performance of the EPMA [32]. The details were presented in the Supporting Information.

2.7. Cell scratch assay

3 T3-L1 cells (2×10^5/well) were seeded into a 6-well plate and cultured for 24 h. Meanwhile, lipopolysaccharide (LPS, 10 μg mL^{-1}) was introduced and the cells were incubated for another 2 h. After that, a sterile pipette tip was utilized to create a scratch in the cell monolayer. The unattached cells were then removed by washing with PBS, and various hydrogels were applied to the cells. Finally, cell images were acquired with fluorescence microscopy and analyzed by Image J

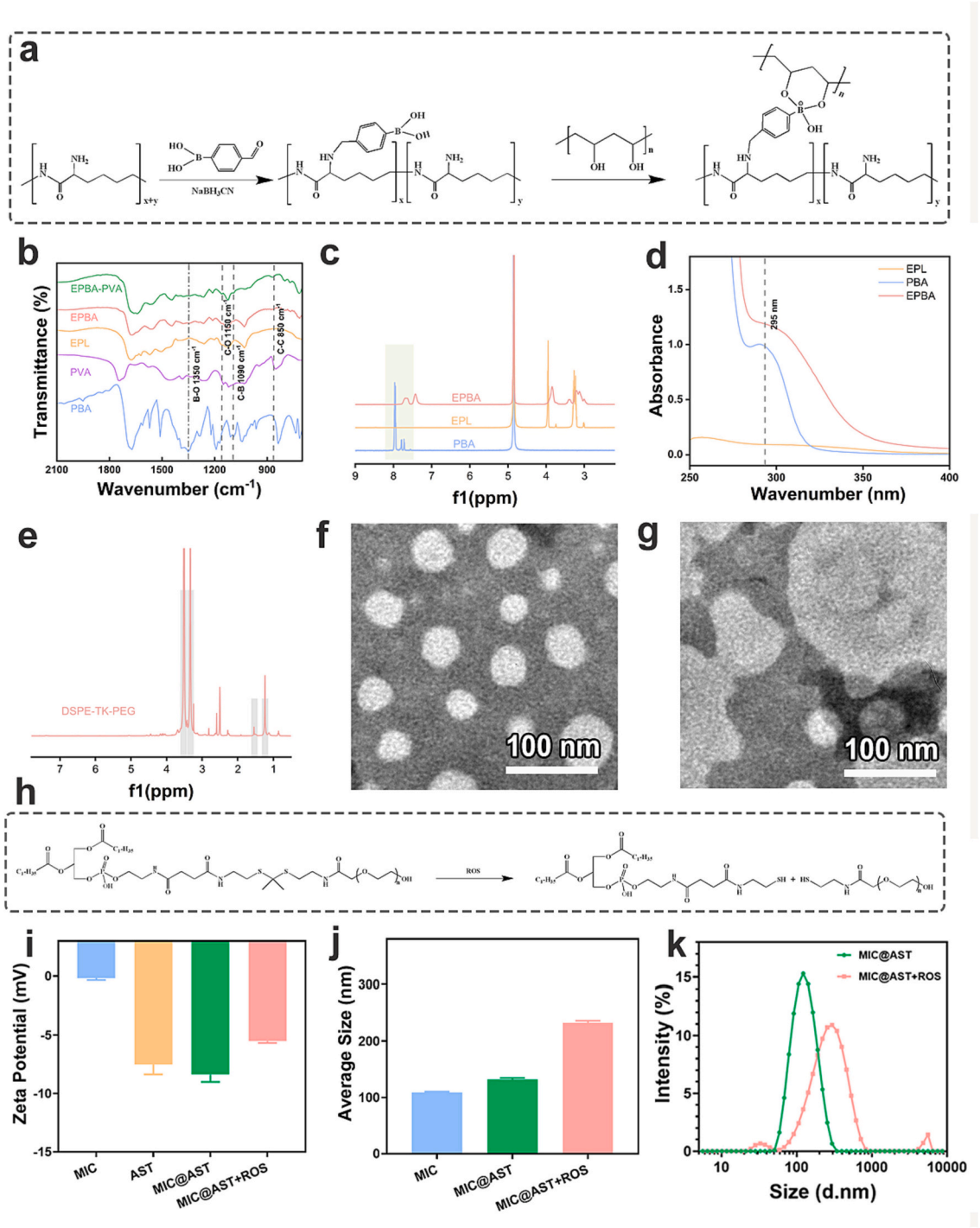

Fig. 1. (a) Schematic illustration of the fabrication of EPBA-PVA hydrogel. (b) FTIR spectra of PBA, EPL, PVA, EPBA and EPBA-PVA hydrogel. (c) ^{1}H NMR spectra of PBA, EPL and EPBA. (d) UV spectra of PBA and EPBA. (e) ^{1}H NMR spectrum of DSPE-TK-PEG. (f) TEM image of MIC&AST. (g) TEM image of MIC&AST treated with H_2O_2. (h) Schematic illustration of ROS-responsive MIC&AST. (i) Zeta potential of MIC, AST, MIC&AST and MIC&AST treated with ROS. (j) Average size of MIC, AST, MIC&AST and MIC&AST treated with ROS. (k) Particle size distribution of MIC&AST and MIC&AST treated with ROS.

software.

2.8. The anti-inflammatory effects of the EPMA and the transformation of macrophages phenotype

LPS-induced RAW 264.7 cells were utilized to explore the anti-inflammatory effects of the EPMA through enzyme-linked immunosorbent assay (ELISA) and immunofluorescent staining. Flow cytometry and immunofluorescent staining were conducted to investigate the transformative effect on macrophage phenotype of EPMA. The details were presented in the Supporting Information.

2.9. Angiogenesis efficiency of the EPMA

To determine the effect of the EPMA hydrogel on angiogenesis, HUVECs were applied to test the vascularization of EPMA through transwell assay, tube formation, ELISA, and immunofluorescent staining. The details were shown in the Supporting Information.

2.10. In vivo wound healing assessment of the EPMA

An animal model of *S. aureus*-infected full-thickness skin was constructed to explore the wound repair performance of hydrogel. In detail, Sprague-Dawley rats weighing 250–300 g were applied to established a standardized full-thickness wound using a round punch with a diameter of 20 mm. Afterwards, rats were then randomly divided into five groups ($n = 5$), and each animal was dropped with 200 μL of *S. aureus* solution. The wound surface was filled with 100 μL of EPMA hydrogel, MIC&AST solution, EPBA-PVA hydrogel, Hydrosorb, or left undressed. Afterwards, the wounds were covered with a sheet of 3 M Tegaderm Film and fixed with bandages, and the dressings were renewed every 3 days. The wounds were captured at different time points to investigate the wound repair effect. To investigate the wound healing period, spread plate method, ELISA, histology analysis, immunofluorescence, and immunohistochemistry staining were carried out. The details were presented in the Supporting Information.

2.11. Statistical analysis

Results are expressed as the mean ± standard deviation. Student's *t*-test and one-way ANOVA was used for statistical analysis. NS represent no significant difference. Statistical significance was defined as a *p*-value less than 0.05.

3. Results and discussion

3.1. Fabrication and characterization EPBA polymer and MIC&AST micelle

The fabrication process of EPBA is shown in Fig. 1**a**. The structure of EPBA was characterized by FTIR, ^{1}H NMR and UV. In the FTIR spectrum of EPBA (Fig. 1**b**), the peaks at 1350 and 1090 cm^{-1}were attributed stretching vibration peak of B − O and B − C respectively. The peaks at 1150 and 850 cm^{-1} in the FTIR spectrum of PVA and EPBA-PVA were attributed as the C − O and C − C stretching vibration of PVA respectively. As shown in Fig. 1**c**, two main characteristic peaks at 7.42 and 7.66 ppm were assigned as hydrogen on the aromatic ring of phenylboronic acid. The characteristic carbon peaks (128.5–134.6 ppm) of aromatic ring on phenylboronic acid were also detected on the ^{13}C NMR spectrum of EPBA compared with that of EPL (Fig. **S1**). As shown in Fig. **S2**, the characteristic peaks of phenylboronic acid on PBA and EPBA were identical, which indicated the presence of phenylboronic acid on EPBA. In addition, the UV spectrum of EPBA (Fig. 1**d** and **S3**) also indicated the absorbance band (295 nm) of phenylboronic acid. The results of FTIR, NMR and UV verified the introduction of phenylboronic acid of EPL and the grafting rate of PBA was approximately 32.6%. The structure of DSPE-TK-PEG was characterized by ^{1}H NMR (Fig. 1**e**). The peaks at 3.36 and 1.54 ppm were corresponded to TK bonds, which is in accordance with previous literature [33]. In addition, the characteristic peaks at 3.55 ppm and 1.25 ppm were attributed to PEG block and DSPE block, respectively. The loading efficiency of AST was determined by HPLC and calculated to be around 27.4% (Fig. **S4**). The micelle exhibits ROS-sensitivity due to the presence of TK bond (Fig. 1**h**). TK is a subclass of the thioether group, which is cleaved to a thiol-containing group and acetone upon exposure to ROS, while being considered biodegradable, non-toxic and amenable to incorporation into other polymers or conjugates [34]. In detail, the first oxidation step occurs at the thioether unit of TK bond, which triggers the functional group degradation to form a sulfenic acid intermediate and a thiocarbenium ion intermediate. Hydrolysis of the latter produces the corresponding thiol, which rapidly reacts with the sulfenic acid to produce a disulfide-based byproduct [35]. Thioketal was a group sensitive to ROS, while insensitive to acid-, base-, protease and reducing environments. Since higher levels of intracellular ROS are generated constantly in chronic wound, thioketal linkers could be specifically cleaved by ROS and respond to the wound ROS micro-environment instead of pH microenvironment [36]. Therefore, the micelles (MIC&AST) will break down under high ROS levels in chronic refractory wounds to release loaded drugs. As shown in Fig. 1**f**, TEM image of MIC&AST indicated that the highly uniform nanoparticles were prepared successfully, and the morphology of MIC&AST collapsed to irregular shape under ROS condition (Fig. 1**g**). The zeta potential (Fig. 1**i**) of micelles converted from −0.18 mV (MIC) to −8.39 mV (MIC&AST) and the average size (Fig. 1**j**) of micelles increased from 108.37 nm (MIC) to 131.63 nm (MIC&AST), which also indicated the encapsulation of AST. Moreover, the zeta potential and average size of MIC&AST markedly increased after under ROS condition, and new curves were also observed in the size distribution of MIC&AST after treated with ROS (Fig. 1**k**). Conclusively, a ROS-responsive MIC&AST was successfully prepared, which was further applied in fabrication of therapeutic hydrogel in the next step.

3.2. Fabrication, characterization and mechanical properties of the EPBA-PVA and EPMA hydrogels

The EPMA hydrogel was prepared by mixing the EPBA@MIC solution (containing 500 μg mL^{-1} MIC&AST) with the PVA solution (Fig. 2**a**). The uniform porous structure of the EPBA-PVA and EPMA hydrogels were observed by SEM (Fig. 2**b** and **S5**), which are beneficial to drug loading and cell recruitment. In addition, the homogeneous distributions of C, N, O, B, S were investigated by EDS analysis (Fig. 2**b** and **S6**), which further verified the formation of a homogeneous structure and successful encapsulation of AST. Swelling and degradation behavior are the essential properties of hydrogel wound dressing, because the former property could ensure the hydrogel absorb the wound exudates and prevent the growth of bacteria, while the latter could make the hydrogel more compatible with the biological healing process [19]. As illustrated in Fig. 2**c**, both of the EPBA-PVA and EPMA hydrogels exhibit high water retention. The swelling ratio increased rapidly within the first 6 h and reached equilibrium within 12 h. Moreover, the swelling ratio of both hydrogels exhibited a downward trend at 48 h, which is due to the partial degradation of the hydrogel after soaking in a simulated physiological microenvironment for a long time. The in vitro degradation behavior of the hydrogels was revealed in Fig. 2**d**, both of the hydrogels exhibited continuous degradation behavior within 7 days, which is beneficial to the removal of dressings while protecting the new tissue from damage.

The rheological properties of the EPBA-PVA and EPMA hydrogels were measured by a rheometer, storage moduli (G′) reflecting the elastic properties and loss moduli (G″) reflecting the viscous properties of the hydrogel were recorded. The frequency sweep of the hydrogels was shown in Fig. 2**e**, G′ significantly exceeded G″ and displayed a frequency-dependent performance with frequencies varying from 0.1 to 100 rad

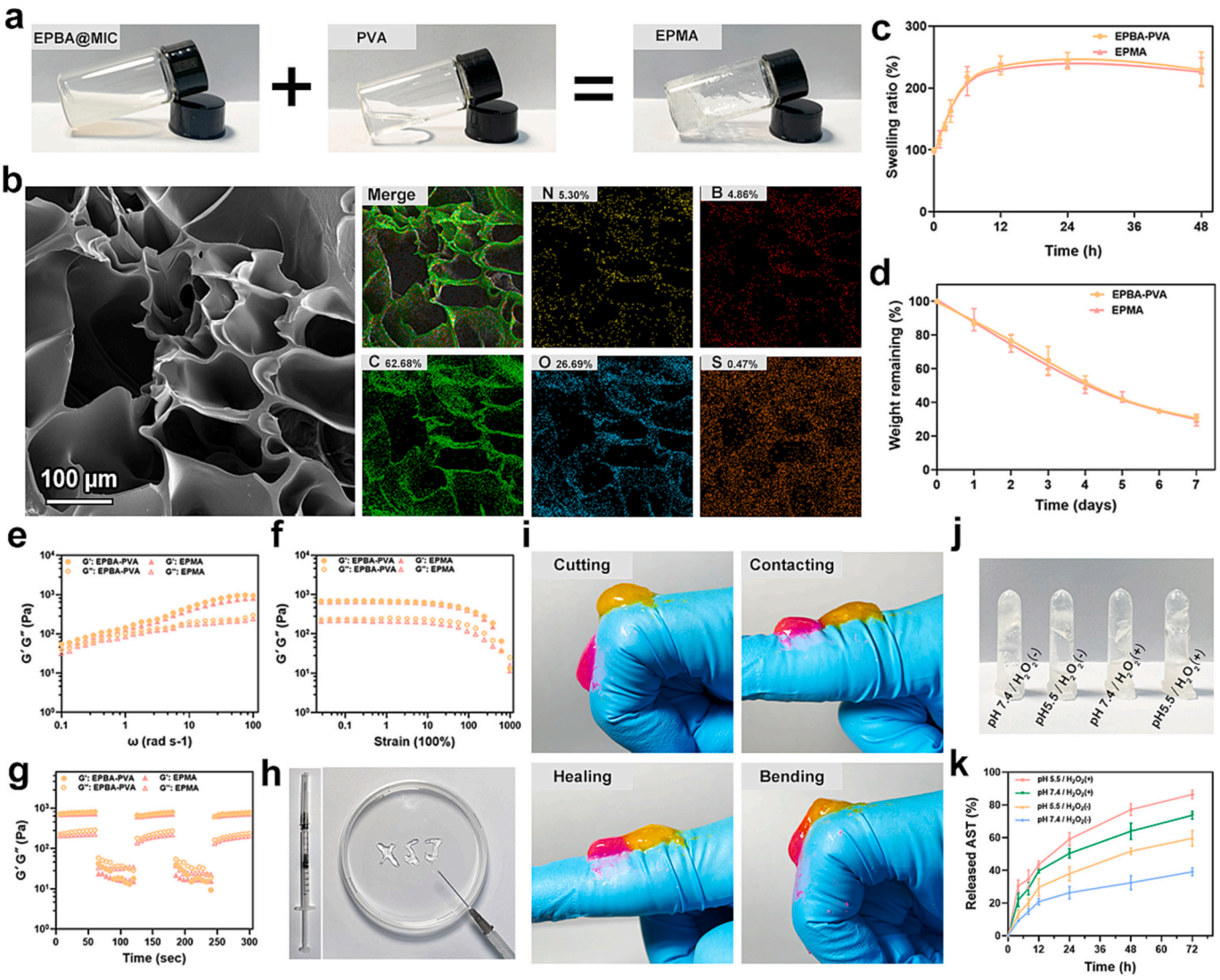

Fig. 2. (a) Gelation photos of the EPMA hydrogel. (b) SEM images and EDS elemental mapping of the EPMA hydrogel. (c, d) Swelling and degradation behavior of the EPMA hydrogel. (e-g) Frequency sweep tests, strain sweep tests and continuous step-strain tests of the EPBA-PVA and EPMA hydrogels. (h) Photographs of EPMA hydrogel of injectability and good writing ability. (i) Self-healing behavior of the EPMA hydrogel. (j-k) pH/ROS dual responsive behavior and AST release kinetics of the EPMA hydrogel.

s^{-1}, indicating the elastic network is formed. Moreover, the rheological properties of both hydrogels w.ere highly similar, which indicate that the hydrogel could still maintain stable rheological properties after the introduction of MIC&AST. As shown in Fig. 2**f**, the G″ values surpassed the corresponding G′ values at 1000% of applied strain, indicating the disintegration of the hydrogels. And then a continuous step strain test (strain between 1% and 1000%) were carried out. As evidenced by Fig. 2**g**, the hydrogels experienced a significant decrease in G' and G" under a 1000% applied strain, with G" outperformed G'. After two cycles, G' and G" quickly returned under a 1% applied strain, indicating that the hydrogels demonstrated remarkable self-healing capabilities.

3.3. Mechanical properties of the hydrogels

An adequate mechanical strength is important for a hydrogel dressing to avoid the breakage caused by body movement. Therefore, the compression and testing properties of the hydrogels have been investigated. As shown in Fig. **S8**, the compressive strength of EPBA-PVA and EPMA hydrogels was approximately 22 kPa at a high strain of 80%. Meanwhile, the load-unload compression stress-strain curves indicated that the hydrogel could withstand a high compression strain of 80% without fracture. Meanwhile, the tensile testing of the hydrogel was further performed. As shown in Fig. **S9**, the results of Young's modulus showed no significant difference between the EPBA-PVA and EPMA hydrogel groups, and the elongation at the break of the two groups remained as high as over 400%. Taken together, all the above results demonstrated that the hydrogel exhibited superior mechanical strength, which have the potential to meet the mechanical needs of soft tissues related applications.

3.4. Adhesion properties of the hydrogels

The lap shear tests were applied to investigate the tissue adhesive properties of the hydrogels to porcine skins. As shown in Fig. **S10**, the adhesion strength of EPBA-PVA and EPMA hydrogel to the porcine skin tissue was approximately 40 kPa, and no significant difference was observed between the two groups, demonstrating that the introduction of MIC&AST had no obvious effect on the adhesion property of hydrogels. In addition, the adhesion property of the EPMA hydrogel was further investigated by tissue adhesion. As shown in Fig. **S11**, the EPMA hydrogel was capable of adhering to major organs including the heart, liver, spleen, lung and kidney without falling out under gravity. Thus,

these results demonstrated that the excellent adhesion of the EPMA hydrogel could provide a stable connection between the wound and the dressing.

3.5. Self-healing, injectable, pH/ROS dual responsive behavior and drug release kinetics of the EPMA hydrogel

The dynamic formation-dissociation cycles of the boronic ester bonds could give the EPMA hydrogel excellent self-healing and injectability properties. As a result, the hydrogel could effectively fill irregular wound beds and quickly repair damaged dressings caused by regular body movements [37]. As presented in Fig. 2**h**, the hydrogel could be continuously injected with a syringe to form the letter "XSJ", indicating the good injectability of the EPMA hydrogel. Thereafter, the EPMA hydrogel was cut into pieces and dyed in various colors to investigate its macroscopic self-healing ability. As depicted in Fig. 2**i**, the dyed EPMA hydrogel pieces were attached to the finger firstly, and then contact with the two pieces for a duration of 2 min, the hydrogel demonstrated the ability to repair itself and withstand the bending force from the finger without exhibiting any cracks.

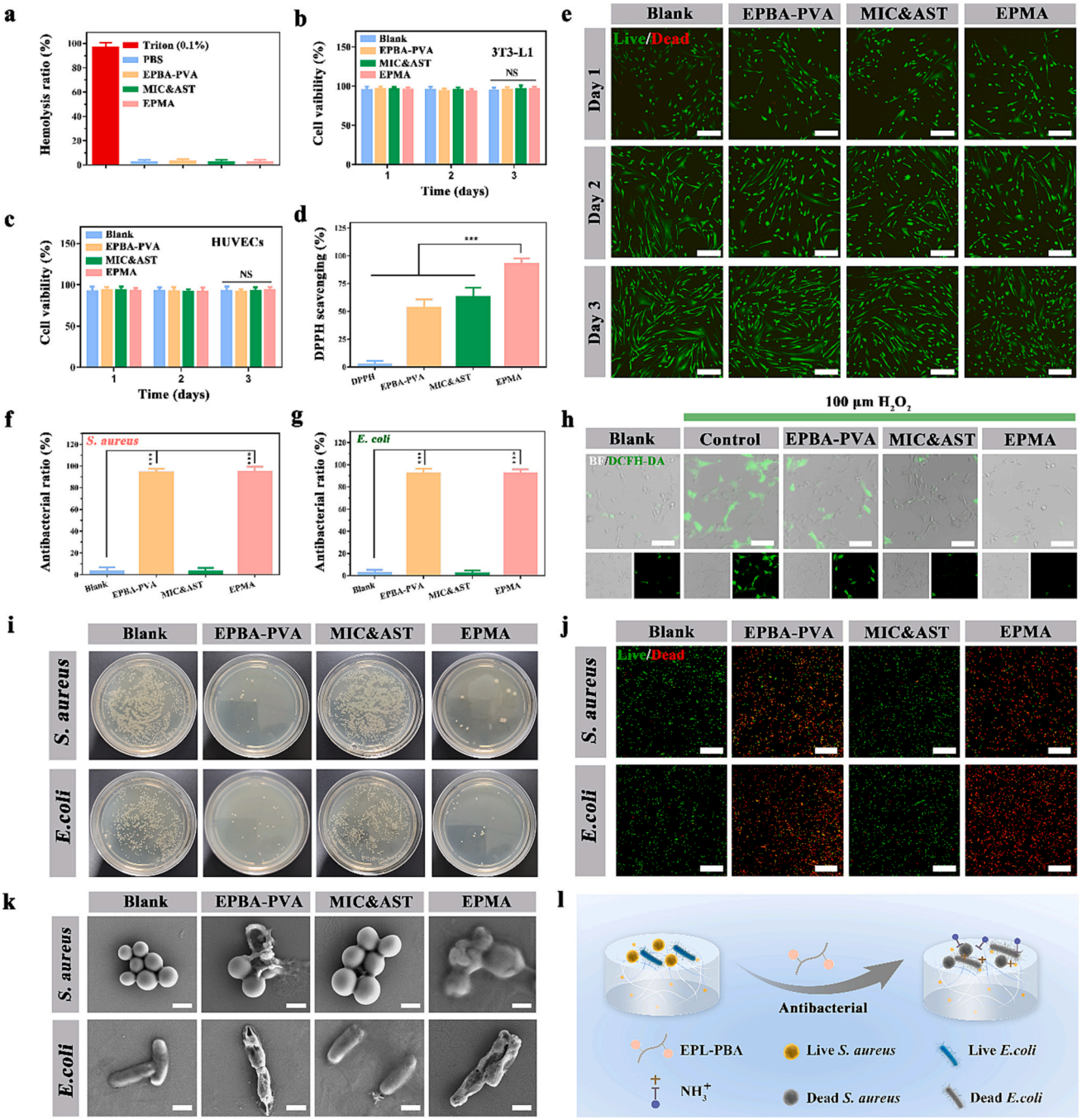

Fig. 3. Biocompatibility properties, antioxidant efficiency, and antibacterial performance of the pH/ROS dual-responsive EPMA. (a) Hemolysis test of different samples ($n = 3$). (b, c) Cell viability of 3 T3-L1 cells and HUVECs after corresponding treatment for 1, 2, and 3 days (n = 3). (d) DPPH scavenging efficiency of different samples (n = 3). (e) Live/dead staining of 3 T3-L1 cells after corresponding treatment (scar bar: 100 μm). (f, g) Antibacterial ratio of different samples (n = 3). (h) Evaluation of intracellular ROS under different hydrogel treatments (scar bar: 50 μm). (i) Digital photographs of bacterial colony formation after corresponding treatment. (j) Live/dead bacterial staining images of *S. aureus and E. coli* after corresponding treatment (scar bar: 50 μm). (k) SEM images of bacterial after corresponding treatment (scar bar: 500 nm). (l) Antibacterial mechanism of the hydrogel.

Generally, when bacterial infection occurs in a chronic wound, the pH of the wound will decrease due to the acidic substances such as lactic acid and carbonic acid generated by bacterial growth [38]. Because the boronic ester bond is easy to break in acidic and oxidizing environment, the EPMA hydrogel exhibited pH/ROS dual responsive behavior (Fig. **S7**). Fig. 2**j** illustrates that upon adding HCl solution (pH 5), the hydrogel gradually disintegrated over a span of 6 h. Similarly, the addition of H_2O_2 (1 mM) elicited a comparable response. These findings suggest that the hydrogel network breaks down due to hydrolysis of the boronic ester bonds when exposed to acidic and oxidative conditions. Once the network collapses, the MIC&AST were exposed to the surrounding environment and then released AST due to the further dissociation of the ROS sensitivity of the TK bonds. Consequently, we analyzed the AST release kinetics of the EPMA under different conditions. As depicted in Fig. 2**k**, in comparison to the control group (26.3%), the amount of released AST increased by 37.9%, 50.4%, and 59.1% after incubating for 24 h at pH 5.5, 100 μM H_2O_2, and pH 5.5 with 100 μM H_2O_2, respectively. This indicates that both pH and ROS functioned as intelligent switches for the EPMA hydrogel, controlling the release of AST. Additionally, AST was continuously and sustainably released over a period of 72 h, which could promote continuous angiogenesis. Overall, the AST release kinetics of the EPMA hydrogel make it highly appropriate for treating chronic wounds characterized by an acidic and oxidizing environment.

3.6. *In vitro biocompatibility of EPMA hydrogel*

As a wound dressing, the biocompatibility of the pH/ROS dual-responsive EPMA hydrogel is of paramount importance for promoting wound repairing [39]. The hemocompatibility of EPMA hydrogel was examined with mouse erythrocyte using Triton X-100 as the positive control, and the results indicated that no significant hemolysis was noted in all experimental groups (Fig. 3**a** and **S12**), demonstrating that the EPMA hydrogel had superior blood compatibility [40]. Fibroblasts cells and endothelial cells were the primary cell types in promoting tissue repair and regeneration, acting an important role in the process of wound repairing. Thus, 3 T3-L1 and HUVECs were used to detect the cytotoxicity of the hydrogel. To further investigate the cytocompatibility of the hydrogel, CCK-8 kit and live/dead staining were conducted. After co-incubation with HUVECs and 3 T3-L1 cells for 3 days, the cell viability of hydrogels was greater than 90%, and no significant difference was found among the four groups (Fig. 3**b** and **c**). In addition, the results of Live/Dead staining revealed that large green fluorescent dots were observed in all groups (Fig. 3**e** and **S13**), reconfirming the favorable biocompatibility of EPMA hydrogel.

3.7. *Antioxidant capacities and antibacterial properties of EPMA hydrogel*

Reactive nitrogen and oxygen species (RNOS) is essential for maintaining the redox homeostasis of the intracellular environment. Specifically, excessive RNOS accumulation can result in long-term inflammation and hinders the progression of skin regeneration owing to the disrupted immune microenvironment in chronic wound [41–43]. Furthermore, excessive RNOS could interfere with signaling cascades and destroy cells, leading to severe irreversible and permanent damage of tissues. Owing to the resulting disproportion between degradation and remodeling processes, chronic wounds persist in the inflammatory phase of the normal healing process and often remain non-healing for months or even years. Thus, wound dressings with the ability of scavenging excessive RNOS could relieve wound tissue oxidative stress and stop the vicious circle of inflammation, thereby promoting chronic wound healing. Because of the AST encapsulation and dynamic nature of boronate esters within our system, EPMA hydrogel is anticipated to present prominent antioxidant performance for chronic wound treatment. The antioxidative ability of the EPMA hydrogel in vitro was evaluated by DPPH free radicals scavenging test and ROS scavenging assay. Not unexpectedly, the EPMA hydrogel displayed a significant DPPH scavenging efficiency (Fig. 3**d**), which may be the consequence of the dynamic arrangement of the of boronate ester bond and the released AST from the hydrogel. Moreover, to further evaluate the intracellular ROS scavenging ability, 100 μM H_2O_2 was introduced to 3 T3-L1 cells and incubated with the EPMA hydrogel, which can imitate a pathological oxidative microenvironment of chronic wounds. Besides, 2′,7′-dichlorofluorescin diacetate (DCFH-DA) also was utilized as a probe to evaluate the intracellular ROS levels. Obviously, the EPMA hydrogel group exhibited remarkably lower intensity of fluorescent signals than the other experimental groups (Fig. 3**h**), demonstrating that the EPMA possessed excellent antioxidative property. Together with the above results, the EPMA hydrogel could be used as a trustworthy wound dressing to eliminate overexpressed RNOS in chronic refractory wounds, which might be beneficial for skin regeneration.

Repeated bacterial infection is a common complication of chronic refractory wounds [23,44], which could prolong the wound healing. Accordingly, wound dressings with intrinsic antibacterial property are important for clinical application [45]. The antibacterial effects of the EPMA hydrogel were comprehensively investigated using *S. aureus* and *E. coli*, which are the main pathogenic bacterium causing chronically infected wounds [46]. First, the antibacterial ratios of the EPMA were assessed by the OD 600 method. As illustrated in Fig. 3**f** and **g**, the EPMA hydrogel indicated superior antibacterial performance for both *S. aureus* (95.3%) and *E. coli* (91.6%), which may be ascribed to the release of EPBA. Meanwhile, the introduction of MIC&AST had no influence on the antibacterial property of the EPMA. Afterward, plate counting method was applied to detect the antibacterial activities of the EPMA. As expected, EPMA hydrogel demonstrated significant antibacterial ability against both *S. aureus* and *E. coli* (Fig. 3**i**). In addition, the images of a live/dead bacterial viability assay indicated that there was a significant presence of dead bacterial (red) in the EPMA hydrogel group (Fig. 3**j**), further indicating good inhibition effects against *S. aureus* and *E. coli*. Finally, the morphology of bacterial after corresponding treatment was evaluated by SEM. As presented in Fig. 3**k**, the membrane depression and rupture of *S. aureus* and *E. coli* was observed, indicating the outstanding antibacterial performance of EPMA hydrogel. The antibacterial mechanism might be ascribed to the fact that EPMA hydrogel could dynamically generate NH_3^+ (Fig. 3**l**), which could destroy the cell membrane of bacteria [47–49], eventual causing bacterial death. Thus, the above results collectively suggested that EPMA hydrogel possessed superior antibacterial effects, indicating their broad application prospects in wound dressings.

3.8. *In vitro cell migration, anti-inflammatory performance and immunological regulation of EPMA hydrogel*

Cell migration play a crucial role during the tissue remodeling process. Thus, scratch assay was performed to detect the effects of EPMA hydrogel on the cell migration behavior, and LPS-activated 3 T3-L1 cells were utilized to simulate wound inflammation in vitro [50]. Notably, the migration of 3 T3-L1 cells was significantly inhibited following the addition of LPS (Fig. 4**b** and **S14**). Meanwhile, compared to other experimental group, the cell migration was significantly enhanced in the EPMA hydrogel group, primarily driven by the antioxidant ability of AST and boronate ester bond. Macrophages is recognized as important immune cells, playing an important role in immunomodulation and skin regeneration [51]. Thus, it is of particular importance to develop wound dressings which possess capability of promoting macrophage polarization toward M2 phenotypes to recover immune homeostasis during tissue remodeling. Therefore, macrophage polarization was further detected by ELISA to evaluate the in vitro anti-inflammatory property of the EPMA hydrogel. LPS stimulation leads to the activation of Raw 264.7 macrophages into the proinflammatory M1 phenotype, which selected as the positive control. After coculture for 24 h and 48 h, results from

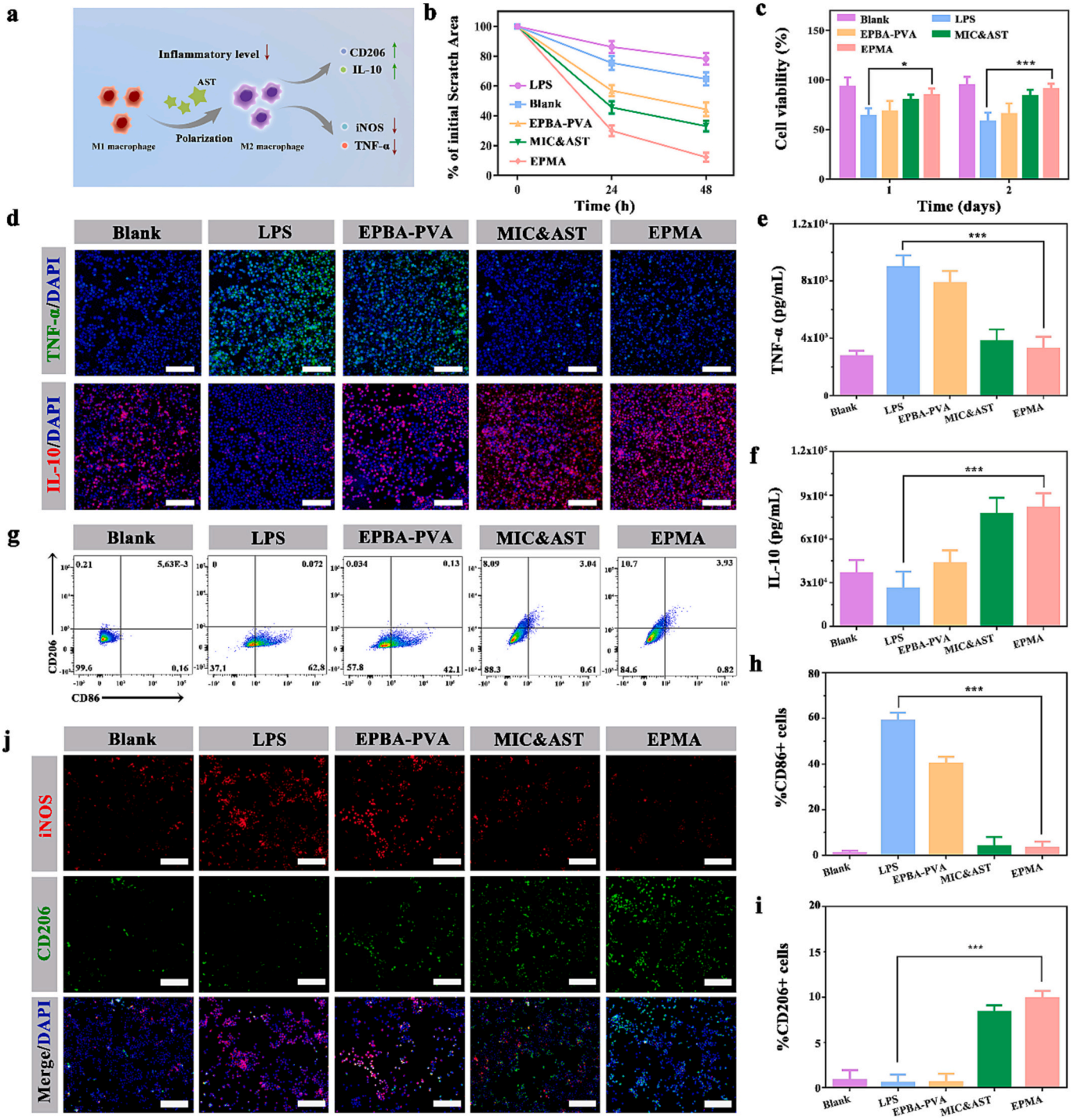

Fig. 4. Effects of EPMA hydrogel on cell migration, macrophage polarization and inflammation amelioration. (a) Schematic demonstrating the roles of EPMA hydrogel in regulating inflammation. (b) Quantification of 3 T3-L1 cells migration ($n = 3$). (c) Cell viability of RAW 264.7 cells treated with different samples (n = 3). (d) Immunoflurescence staining for TNF-α and IL-10 after corresponding treatment (scar bar:100 μm). (e, f) The expression level of TNF-α and IL-10 with the different treatment (n = 3). (g-i) Flow cytometry and quantification of CD206 and CD86 expression (n = 3). (j) Immunofluorescence staining for iNOS and CD206 in RAW 264.7 cells treated with different samples (scar bar: 100 μm).

CCK-8 demonstrated that the cell viability increased remarkably in the EPMA hydrogel group (Fig. 4**c**), which might be attributed to the EPMA inhibiting inflammation of macrophages. Furthermore, the results of ELISA assay indicated that TNF-α expression was remarkably down-regulated in the EPMA hydrogel-treated group, while the IL-10 expression in the EPMA hydrogel-treated group was remarkably upregulated when compared with the blank group (Fig. 4**e** and **f**). Furthermore, the results of immunofluorescence staining indicated that TNF-α labeled green fluorescence was significantly decreased and IL-10 labeled red fluorescence was remarkably increased in inflammatory cells after EPMA hydrogel treatment (Fig. 4**d**), suggesting enhanced anti-inflammation.

Macrophages can differentially polarize into pro-inflammatory (M1) and anti-inflammatory phenotypes (M2) and play a key role in regulating the immune response and accelerating tissue remodeling in chronic wounds [12,52] (Fig. 4**a**). The failure of macrophages to switch

phenotypes from M1 to M2 has been associated with delayed wound healing and chronic inflammation [53]. Hence, the immunofluorescence staining and flow cytometry analysis were carried out to explore the immune regulation of hydrogels. Flow cytometry analysis indicated that the ratio of $CD86^+$ macrophages remarkably increased following the addition of LPS (Fig. 4**g**). However, a significantly reduced ratio $CD86^+$ and a marked increased ratio of $CD206^+$ were noted after EPMA hydrogel treating (Fig. 4**h** and **i**). Meanwhile, the immunofluorescence staining images indicated that the iNOS expression was remarkably reduced following EPMA hydrogel treatment, whereas the CD206 expression was significant increased (Fig. 4**j**). In addition, the EPMA hydrogel treated group exhibited a remarkably lower iNOS fluorescence intensity, whereas the fluorescence intensity of CD206 was increased compared to the other groups, demonstrating the enhanced polarization of M2 macrophage (Fig. **S15**). Accordingly, all the above results indicate that EPMA hydrogel could regulate immune microenvironment by polarizing macrophages from M1 to M2 phenotype and could potentially accelerate the skin repair by inhibiting the expression of inflammatory cytokines.

3.9. Mechanism of EPMA hydrogel promoting chronic wound healing

To further investigate the regulatory effect and potential mechanism of the EPMA hydrogels on macrophages, RNA sequencing (RNA-Seq) was conducted. The Venn diagram shows that 706 genes were expressed in only untreated cells, and 608 genes were expressed in EPMA-treated cells (Fig. 5**a**). Differentially expressed genes (DEGs) analysis and volcano plot indicated that 117 genes were upregulated and 111 genes were downregulated in EPMA hydrogel group (Fig. 5**b** and **c**). The gene expression heatmap also demonstrated DEGs between the control and EPMA groups (Fig. 5**d**). Gene enrichment (GO) enrichment analysis of the RNA-seq showed that EPMA hydrogel-treated group changed the molecular function, cellular component, and biological process (Fig. 5**e**), and most of alterations were significantly enriched in immune system, indicating that EPMA hydrogel may improve wound healing through immunoregulation. Consistently, gene set enrichment analysis (GSEA) indicated significant downregulation of the "NOD-like receptor" and "TNF pathways", further demonstrating the role of EMPA hydrogel in the immune response (Fig. 5**f**). Meanwhile, Kyoto Encyclopedia of Genes and Genomes (KEGG) pathway enrichment analysis revealed that EPMA hydrogel affected the NF-kappa B, TNF pathway, and other inflammation-related pathways (Fig. 5**g**). Previous studies have proved that activating the IL-17 pathway triggered the release of pro-inflammatory cytokines, contributing to M1 macrophages polarization, which is closely related to the deterioration of chronic refractory wounds. In particular, the EMPA hydrogel-treated group relieve the damage induced by chronic wounds though the inhibition of IL-17 pathway. Moreover, a quantitative real-time PCR (RT-qPCR) assay further confirmed the excellent anti-inflammatory ability of EPMA hydrogel, as the expression levels inflammation-related genes (IL-6, TNF, CCL2, IL-1b) were significantly reduced in the EPMA group (Fig. **S16**). Overall, the EPMA hydrogel could act as an immune-regulating platform which relieve inflammation by inhibiting the NF-kappa B pathway, which inducing the macrophage transformation from M1 to M2 phenotype, thus accelerating tissue regeneration.

3.10. Angiogenesis efficiency of EPMA hydrogel

The ability to accelerate the formation of blood vessels is indispensable for the wound dressing because abundant neovascularization provides scaffolds for collagen decomposition in chronic wounds and expedite tissue regeneration [54]. In chronic wounds, vascular occlusion is one of the major reasons for delayed wound healing [55]. Thus, inducing neovascularization are critical for accelerating chronic wound healing [56]. Neovascularization is associated with the recruitment of vascular endothelial cells [57], and transwell assay was carried out to investigate the impact of the EPMA hydrogel on the endothelial cell migration. As shown in Fig. 6**a**, the results of transwell assay showed that HUVECs treated with MIC&AST and EPMA exhibited faster migration rates. In the wound healing process, angiogenesis is highly correlated with growth factors secreted by vascular endothelial cells, including VEGF and HIF-1α. Therefore, ELISA and immunofluorescence staining were performed to evaluate the expression levels of VEGF and HIF-1α after treating with different samples. As presented in Fig. 6**c** and **d**, the results of ELISA suggested that VEGF and HIF-1a expression in the EPMA group was remarkably higher than the control group. Moreover, immunofluorescence staining of VEGF and HIF-1α indicated that EPMA hydrogel could promote angiogenesis in chronic wounds (Fig. 6**b**). This phenomenon could be ascribed to the sustained release of AST. It has been reported that AST exerted a dose-dependent manner in promoting blood vessels formation [58]. Hence, we further evaluated the vessel-forming ability of HUVECs treated in EPMA hydrogel through a tube formation assay. Notably, HUVECs exhibited more junctions and longer lengths within the range of 0–80 μmol/L, while an evident decrease in tube formation was noted when the AST concentration achieved 160 μmol/L (Fig. **S17** and **S18**). Notably, it could be observed that the total tube length evaluated after 24 h in EPMA hydrogel group was remarkably higher than other groups (Fig. 6**e-g**). Collectively, the above results demonstrated that the EPMA hydrogel significantly accelerated the formation of blood vessels and increased the expression of cytokines associated with neovascularization, thus making earlier vascularization possible in skin repair.

3.11. In vivo wound healing assessment

The degradation properties of EPMA hydrogel in vivo are important for biomaterials and tissue engineering. Under the skin of rats, a complete hydrogel construct was formed after 0.5 h of injection (Fig. **S19**). Afterwards, the hydrogel construct decreased gradually in size and mass days after subcutaneous implantation within 7 days, while at the wound site of rat, such hydrogels also exhibited a similar degradation rate, demonstrating the rapid degradation of EPMA hydrogels in vivo. To further determine the abilities of the EPMA hydrogel to accelerate chronic wound healing, an infected cutaneous wound model was established by us [50,59] (Fig. 7**a**). The process of skin repairing of the full-thickness in different groups were observed through representative images at day 0, 7, 14, and 21. On the 21th day, the wound closure rates were respectively 64.6% for the MIC&AST group, 84.9% for the EPBA-PVA group, and 94.7% for the EPMA group, while only 49.8% for the blank group, and 56.6% the hydrosorb group (Fig. 7**b, c** and **g**). Notably, the wound in the EPMA hydrogel group was basically healed, whereas there were still visible scars observed in other experimental group after 21 days of treatment. To further evaluate the antibacterial properties of the EPMA in vivo, plate counting method was performed to evaluate the residual bacterial in the wound area on day 7. As depicted in Fig. 7**d** and **h**, many bacteria survived on the wounds in the blank, hydrosorb, and MIC&AST groups, while significantly fewer bacterial colonies were noted in the EPBA-PVA and EPMA hydrogel group. Thus, the above results revealed that the EPMA hydrogel could significantly inhibiting bacterial infection, which was ascribed to the intrinsic antibacterial property of the hydrogel.

To further investigate the effects of EPMA hydrogel on promoting wound repair in different stages, histological analysis was performed on the regenerated skin tissues. The results in Fig. 7**e, i** and **S21** showed that the groups treated with EPMA hydrogel exhibited a significantly reduction of wound length compared to the other experimental groups. In addition, the process of collagen deposition in wound sites were further explored by Masson's trichrome staining (Fig. 7f, j and **S21**). Notably, the EPMA hydrogel group exhibited the densest collagen deposition, further demonstrating that the EPMA hydrogel promoted the skin repair by accelerating collagen deposition.

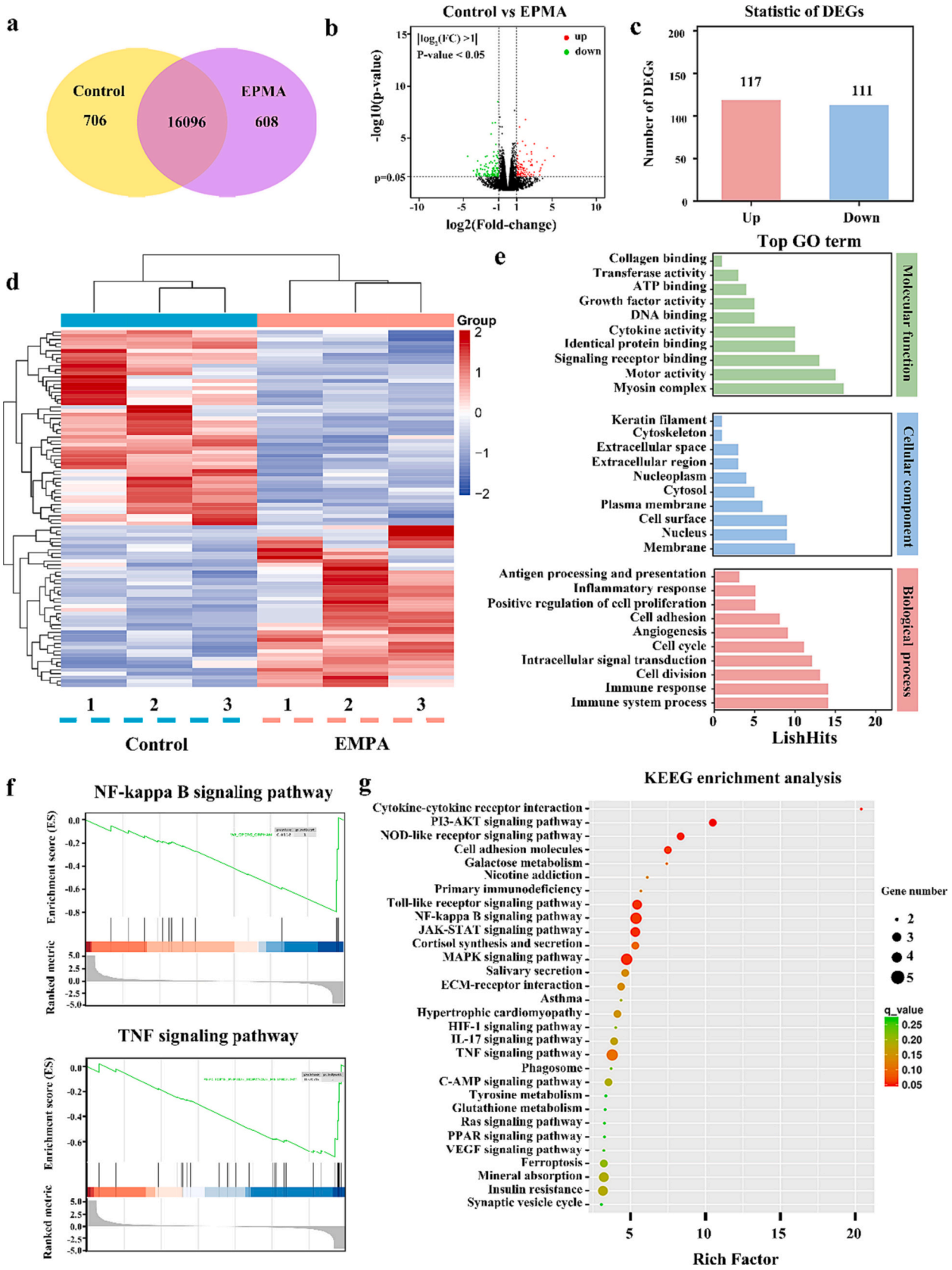

Fig. 5. Evaluation of RNA sequencing results after treatment with EPMA. (a) Venn diagram of the gene characteristics of RAW 264.7 cells. (b) Volcano plots illustrating the upregulated and downregulated genes in response to EPMA treatment. (c) The number of upregulated and downregulated genes. (d, e) Heatmap representation and GO enrichment analysis of the DEGs. (f) GSEA presenting the DEGs within the KEGG pathway. (g) KEGG pathway enrichment analysis of the DEGs.

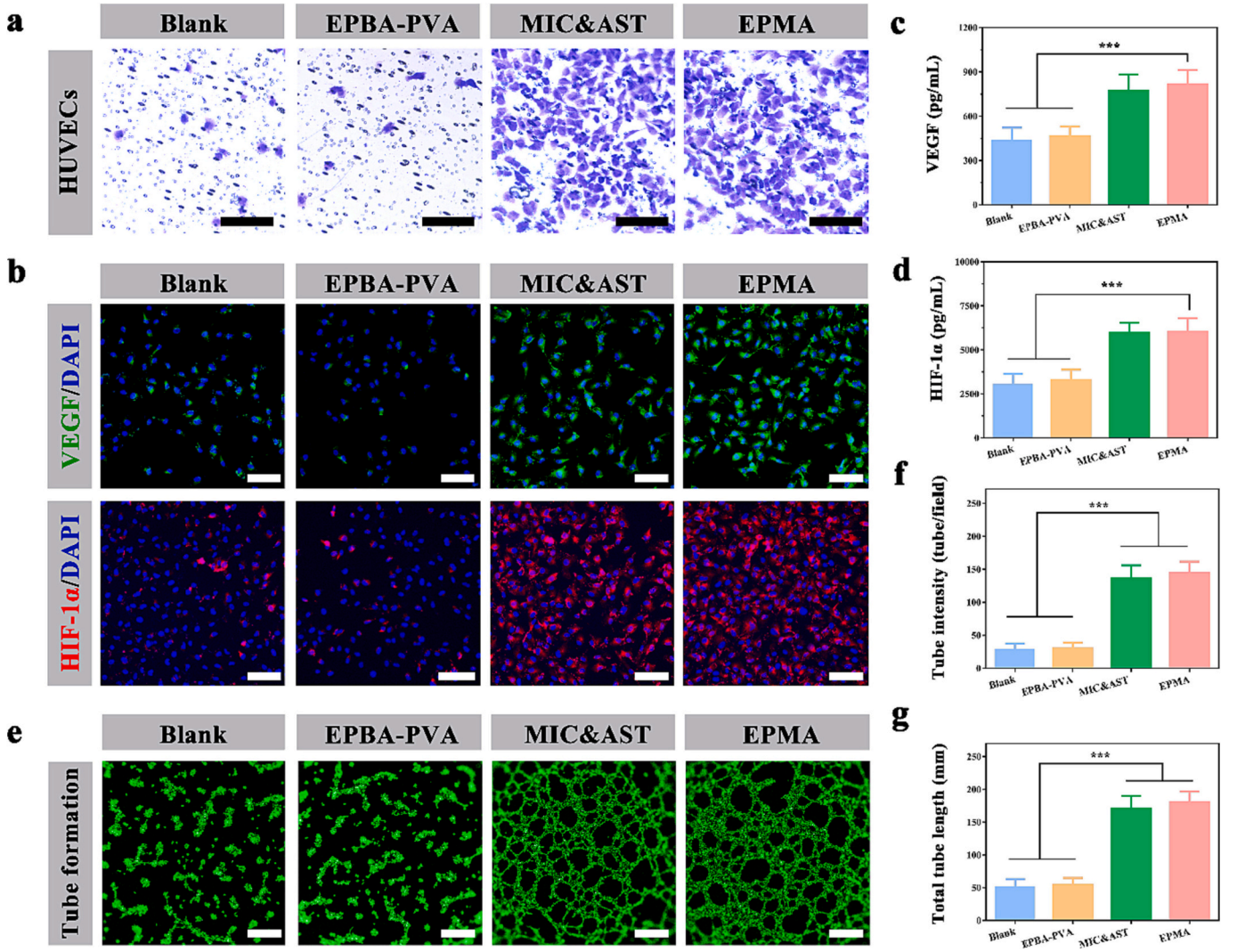

Fig. 6. Angiogenic properties of EPMA hydrogel. (a) Transwell assay of HUVECs following treatment with different samples (scar bar: 50 μm). (b) Representative images of VEGF and HIF-1α immunofluorescence staining after corresponding treatment (scar bar: 50 μm). (c, d) VEGF and HIF-1α expression levels in different groups ($n = 3$). (e-g) Representative images and quantitative analysis of the tube formation assay in HUVECs (scar bar: 100 μm).

3.12. Histopathologic assessment of wound tissues

Chronic refractory wound typically exhibited persistent inflammation, which is often feature with the accumulation of ROS, overexpression of inflammatory cytokines, and inability transition of macrophages to switch phenotypes from M1 to M2 [60]. The ROS content in the wounds was determined by Dihydroethidium (DHE) staining. As presented in Fig. 8**a** and **S20**, the fluorescence signal of DHE was remarkably decreased in the EPMA hydrogel group, revealing its superior antioxidant abilities. Furthermore, the immunohistochemical staining indicated that, when compared to the other experimental groups, TNF-α expression was remarkably reduced, while IL-10 expression was remarkably increased after treatment with EPMA hydrogel on days 7 and 21 (Fig. **S22** and **8b**), further demonstrating that the excellent ability of EPMA hydrogel inhibit inflammatory response.

It is well-established that sustained inflammation causes hard-to-healing wounds, and the transition from inflammation to the proliferation stage are mainly regulate by M2 macrophage [61]. Moreover, the in vitro results had confirmed that the EPMA could promote the transition of the M1 phenotype toward M2 phenotype, we supposed that the modulation of inflammatory cytokines was associated with the effective transition in macrophage phenotype. On days 7 and 21, the immunofluorescence results indicated that the EPMA group exhibited decreased iNOS and increased CD206 expression (Fig. **S20** and **8a**), which demonstrated a positive transition from M1 to M2 phenotype after treatment with EPMA.

Neovascularization plays an important role in bringing oxygen and nutrients to healing cells and promoting the growth of newly-formed granulation tissue [62]. Hence, the process of angiogenesis is of paramount importance for accelerating wound repair and skin regeneration. To explore the neovascularization in the wound tissues, CD31 and VEGF Immunofluorescence staining was performed. The results revealed that the EPMA hydrogel group remarkably promoted the expression of CD31 and VEGF in regenerated skin, whether on day 7 or day 21 (Fig. **S20** and Fig. 8**a**). Meanwhile, the TNF-α, IL-10, VEGF and CD31 expression levels were further evaluated by ELISA (Fig. 8**c–f**), and the results were comparable to the results of the immunohistochemistry and immunofluorescence staining. Additionally, systematic in vivo toxicity evaluation also indicated that the superior biosafety of EPMA hydrogel (Fig. **S23**). Collectively, the EPMA hydrogel showed promising potential in treating chronic refractory wounds by simultaneously eradicating bacterial, ameliorating oxidative stress, alleviating inflammation, and boosting angiogenesis.

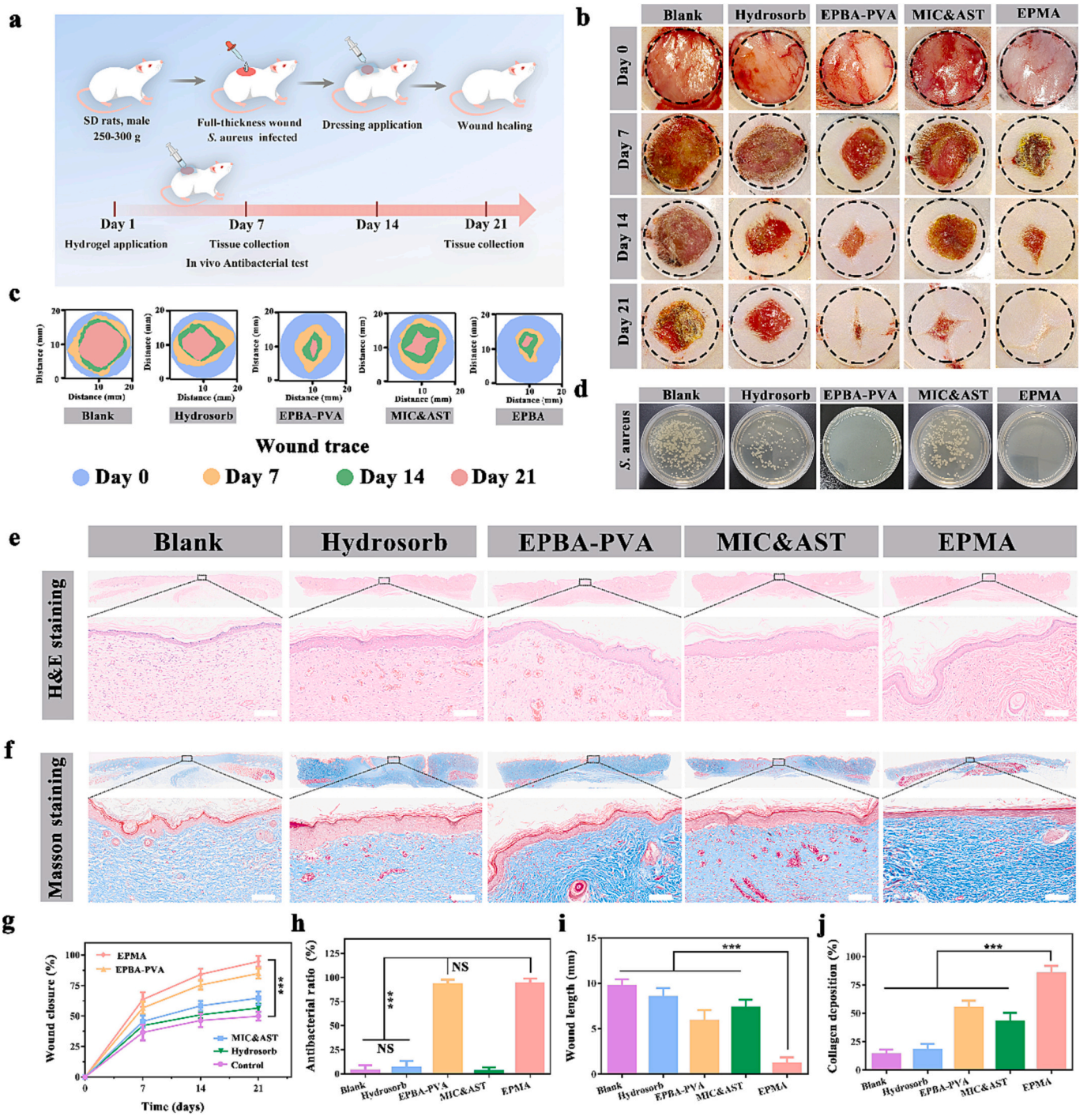

Fig. 7. The efficiency of the EPMA hydrogel in treating infected chronic wounds. (a) Schematic illustration of the timeline of animal experiments to explore the therapeutic effects of hydrogels. (b, c) Representative wound images and simulated wound traces in different groups in 0, 7, 14, and 21 days. (d, h) Photos of bacterial colony formation and in vivo antibacterial ratio after treating with different samples. (e, f) H&E and Masson's trichrome staining of wound tissues on day 21 (scar bar: 100 μm). (g) Quantitative analysis of wound closure in different groups ($n = 3$). (i, j) Wound length and collage deposition in different groups (n = 3).

4. Conclusion

To sum up, we successfully fabricated a multifunctional glycopeptide EPMA hydrogel as an ideal dressing to accelerate skin tissue regeneration and repair in chronic refractory wounds. Owing to the dynamic nature of boronic ester bonds, the hydrogel exhibited effective self-healing ability and pH/ROS responsiveness, which could greatly promote its biomedical application and ameliorate oxidative stress in chronic refractory wounds. Notably, the intelligent hydrogel encapsulated with AST simultaneously exhibited versatile biological activities, such as antibacterial, anti-oxidation, anti-inflammatory, promoting angiogenesis, and regulation of macrophage polarization, which comprehensively contributing to skin repair at multiple phases during the process of chronic wound healing. It offers novel perception to employ Chinese herbal medicine to improve therapeutic effects of chronic wound healing. The results in vivo verified that the EPMA hydrogel could remarkably accelerate wound repairing through eliminating bacterial, hampering oxidative stress, suppressing inflammation,

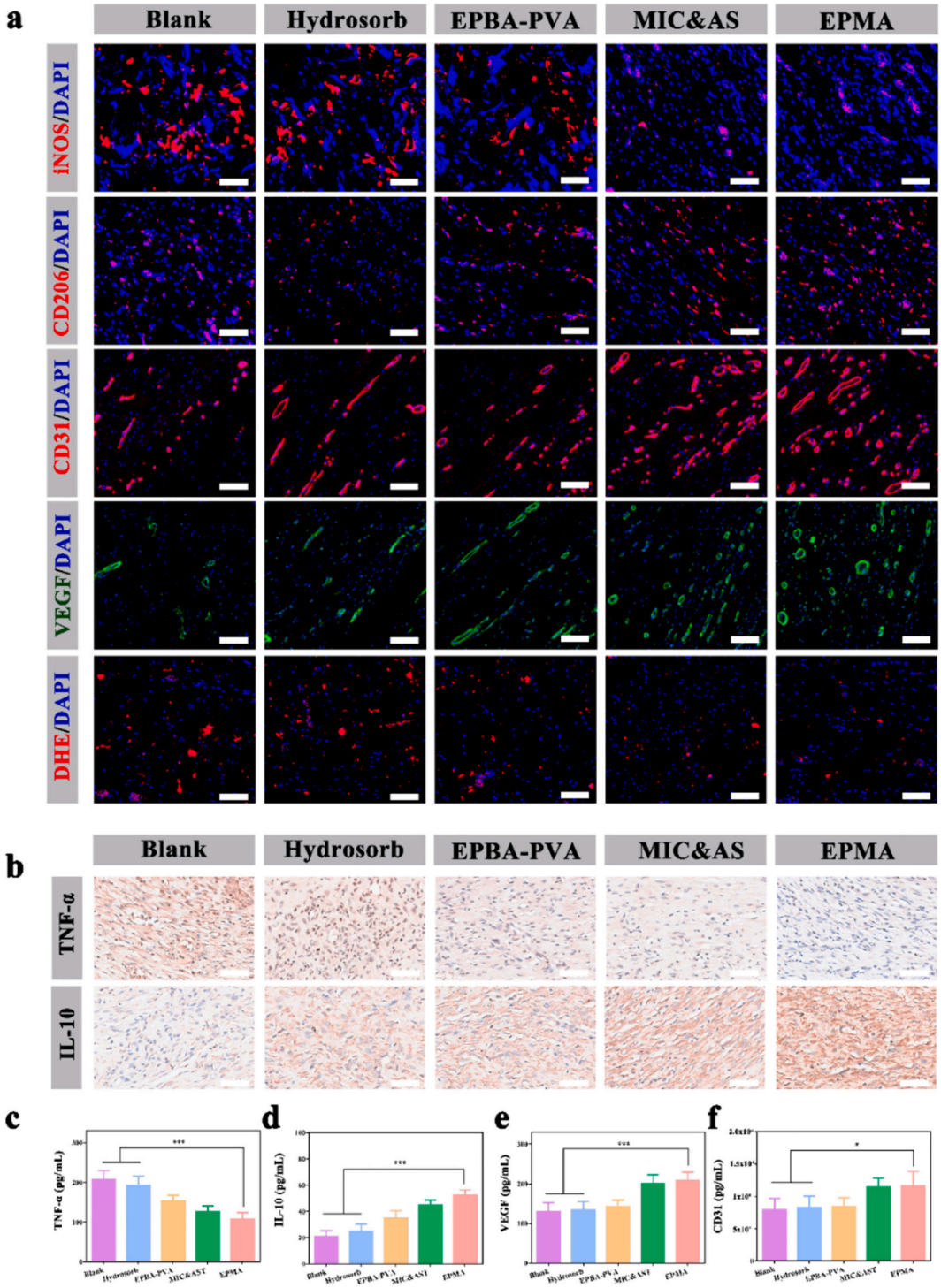

Fig. 8. Histological analysis of the wound tissues. (a) iNOS, CD206, CD31, VEGF, and DHE staining of the wound tissues at days 21 (scar bar: 100 μm). (b) Immunohistochemistry staining of TNF-α and IL-10 in the wound area at days 21 (scar bar: 100 μm). (c–f) The expression of TNF-α, IL-10, VEGF, and CD 31 in the wound tissues at days 21.

promoting angiogenesis and collagen deposition. Taken together, the resulting EPMA with multifunction property regulated the immune microenvironment and promoted skin regeneration. It is an ideal wound dressing and possess remarkable potential for further clinical application and translation inf chronic refractory wounds.

Author contribution

Xiangtian Deng and Ye Wu equally contribution.

Funding

Natural Science Foundation of Sichuan (2023NSFSC1835), Tibet Autonomous Region co-funded project (XZ202301ZY0046G), Post-Doctor Research Project of West China Hospital, Sichuan University (2023HXBH106, 2023HXBH082), China Postdoctoral Science Foundation (2023M742468, 2023M732459, 2023 M732467, 2023TQ0224), Sichuan Science and Technology Program (2023NSFSC1746).

CRediT authorship contribution statement

Xiangtian Deng: Writing – original draft, Visualization, Validation. **Ye Wu:** Writing – original draft, Software, Project administration, Formal analysis. **YunFeng Tang:** Validation. **Zilu Ge:** Software, Resources. **Dong Wang:** Formal analysis, Data curation. **Cheng Zheng:** Writing – review & editing, Visualization, Validation, Conceptualization. **Renliang Zhao:** Writing – review & editing, Validation, Software, Resources, Investigation, Funding acquisition, Formal analysis. **Wei Lin:** Validation. **Guanglin Wang:** Visualization, Supervision.

Declaration of competing interest

There are no conflicts of interest to declare.

Data availability

Data will be made available on request.

Appendix A. Supplementary data

Supplementary data to this article can be found online at https://doi.org/10.1016/j.jconrel.2024.03.002.

References

[1] K. Zheng, Y. Tong, S. Zhang, R. He, L. Xiao, Z. Iqbal, Y. Zhang, J. Gao, L. Zhang, L. Jiang, Y. Li, Flexible Bicolorimetric polyacrylamide/chitosan hydrogels for smart real-time monitoring and promotion of wound healing, Adv. Funct. Mater. 31 (34) (2021).

[2] B. Mirani, E. Pagan, B. Currie, M.A. Siddiqui, R. Hosseinzadeh, P. Mostafalu, Y. S. Zhang, A. Ghahary, M. Akbari, An advanced multifunctional hydrogel-based dressing for wound monitoring and drug delivery, Adv. Healthc. Mater. 6 (19) (2017).

[3] E.S. Chambers, M. Vukmanovic-Stejic, Skin barrier immunity and ageing, Immunology 160 (2) (2020) 116–125.

[4] Y. Cai, K. Chen, C. Liu, X. Qu, Harnessing strategies for enhancing diabetic wound healing from the perspective of spatial inflammation patterns, Bioact. Mater. 28 (2023) 243–254.

[5] V. Falanga, R.R. Isseroff, A.M. Soulika, M. Romanelli, D. Margolis, S. Kapp, M. Granick, K. Harding, Chronic wounds, Nat. Rev. Dis. Primers. 8 (1) (2022).

[6] D.G. Armstrong, T.W. Tan, A. Boulton, S.A. Bus, Diabetic foot ulcers: a review, Jama-J Am Med. Assoc. 330 (1) (2023) 62–75.

[7] J.G. Powers, C. Higham, K. Broussard, T.J. Phillips, Wound healing and treating wounds: chronic wound care and management, J. Am. Acad. Dermatol. 74 (4) (2016) 607–625, 625–626.

[8] E. Bakkeren, M. Diard, W. Hardt, Evolutionary causes and consequences of bacterial antibiotic persistence, Nat. Rev. Microbiol. 18 (9) (2020) 479–490.

[9] W. Liu, R. Gao, C. Yang, Z. Feng, W. Ou-Yang, X. Pan, P. Huang, C. Zhang, D. Kong, W. Wang, ECM-mimetic immunomodulatory hydrogel for methicillin-resistant Staphylococcus aureus-infected chronic skin wound healing, Sci. Adv. 8 (27) (2022) eabn7006.

[10] Y. Qian, Y. Zheng, J. Jin, X. Wu, K. Xu, M. Dai, Q. Niu, H. Zheng, X. He, J. Shen, Immunoregulation in diabetic wound repair with a Photoenhanced Glycyrrhizic acid hydrogel scaffold, Adv. Mater. 34 (29) (2022).

[11] S.A. Eming, T.A. Wynn, P. Martin, Inflammation and metabolism in tissue repair and regeneration, Science 356 (6342) (2017) 1026–1030.

[12] P. Wang, J. Wu, H. Yang, H. Liu, T. Yao, C. Liu, Y. Gong, M. Wang, G. Ji, P. Huang, X. Wang, Intelligent microneedle patch with prolonged local release of hydrogen and magnesium ions for diabetic wound healing, Bioact. Mater. 24 (2023) 463–476.

[13] M. Dougan, G. Dranoff, S.K. Dougan, GM-CSF, IL-3, and IL-5 family of cytokines: regulators of inflammation, Immunity 50 (4) (2019) 796–811.

[14] H. Wu, F. Li, W. Shao, J. Gao, D. Ling, Promoting angiogenesis in oxidative diabetic wound microenvironment using a Nanozyme-reinforced self-protecting hydrogel, ACS Central Sci. 5 (3) (2019) 477–485.

[15] Y. Zhang, R. Sheng, J. Chen, H. Wang, Y. Zhu, Z. Cao, X. Zhao, Z. Wang, C. Liu, Z. Chen, P. Zhang, B. Kuang, H. Zheng, C. Shen, Q. Yao, W. Zhang, Silk fibroin and Sericin differentially potentiate the paracrine and regenerative functions of stem cells through multiomics analysis, Adv. Mater. 35 (20) (2023).

[16] Y. Liu, F. Li, Z. Guo, Y. Xiao, Y. Zhang, X. Sun, T. Zhe, Y. Cao, L. Wang, Q. Lu, J. Wang, Silver nanoparticle-embedded hydrogel as a photothermal platform for combating bacterial infections, Chem. Eng. J. 382 (2020) 122990.

[17] D.E. Bloom, S. Black, D. Salisbury, R. Rappuoli, Antimicrobial resistance and the role of vaccines, Proc. Natl. Acad. Sci. 115 (51) (2018) 12868–12871.

[18] J. Zhao, T. Xu, J. Sun, H. Yuan, M. Hou, Z. Li, J. Wang, Z. Liang, Multifunctional nanozyme-reinforced copper-coordination polymer nanoparticles for drug-resistance bacteria extinction and diabetic wound healing, Biomater. Res. 27 (1) (2023) 88.

[19] Y. Wu, Y. Wang, C. Zheng, C. Hu, L. Yang, Q. Kong, H. Zhang, Y. Wang, A Versatile Glycopeptide Hydrogel Promotes Chronic Refractory Wound Healing through Bacterial Elimination, Immunoregulation, and Neovascularization. ADV FUNCT MATER, Sustained Oxygenation, 2023.

[20] S. Wang, H. Zheng, L. Zhou, F. Cheng, Z. Liu, H. Zhang, L. Wang, Q. Zhang, Nanoenzyme-reinforced injectable hydrogel for healing diabetic wounds infected with multidrug resistant Bacteria, Nano Lett. 20 (7) (2020) 5149–5158.

[21] A.P. Veith, K. Henderson, A. Spencer, A.D. Sligar, A.B. Baker, Therapeutic strategies for enhancing angiogenesis in wound healing, Adv. Drug Deliv. Rev. 146 (2019) 97–125.

[22] F. Wang, H. Qian, L. Kong, W. Wang, X. Wang, Z. Xu, Y. Chai, J. Xu, Q. Kang, Accelerated bone regeneration by Astragaloside IV through stimulating the coupling of osteogenesis and angiogenesis, Int. J. Biol. Sci. 17 (7) (2021) 1821–1836.

[23] S. Lee, W. Chang, Z. Li, N.S. Kirkby, W. Tsai, S. Huang, C. Ou, T. Chang, Astragaloside VI and cycloastragenol-6-O-beta-D-glucoside promote wound healing in vitro and in vivo, Phytomedicine 38 (2018) 183–191.

[24] X. Luo, P. Huang, B. Yuan, T. Liu, F. Lan, X. Lu, L. Dai, Y. Liu, H. Yin, Astragaloside IV enhances diabetic wound healing involving upregulation of alternatively activated macrophages, Int. Immunopharmacol. 35 (2016) 22–28.

[25] R. Yu, H. Zhang, B. Guo, Conductive biomaterials as bioactive wound dressing for wound healing and skin tissue engineering, Nano-Micro Lett. 14 (1) (2021) 1.

[26] G. Chen, Y. Yu, X. Wu, G. Wang, J. Ren, Y. Zhao, Bioinspired multifunctional hybrid hydrogel promotes wound healing, Adv. Funct. Mater. 28 (33) (2018).

[27] M. Kharaziha, A. Baidya, N. Annabi, Rational Design of Immunomodulatory Hydrogels for chronic wound healing, Adv. Mater. 33 (39) (2021) e2100176.

[28] Z. Yang, R. Huang, B. Zheng, W. Guo, C. Li, W. He, Y. Wei, Y. Du, H. Wang, D. Wu, H. Wang, Highly Stretchable, Adhesive, biocompatible, and antibacterial hydrogel dressings for wound healing, Adv. Sci. 8 (8) (2021) 2003627.

[29] W. Liu, R. Gao, C. Yang, Z. Feng, W. Ou-Yang, X. Pan, P. Huang, C. Zhang, D. Kong, W. Wang, ECM-mimetic immunomodulatory hydrogel for methicillin-resistant Staphylococcus aureus-infected chronic skin wound healing, Sci. Adv. 8 (27) (2022) eabn7006.

[30] M. Kharaziha, A. Baidya, N. Annabi, Rational Design of Immunomodulatory Hydrogels for chronic wound healing, Adv. Mater. 33 (39) (2021).

[31] M. Kharaziha, A. Baidya, N. Annabi, Rational Design of Immunomodulatory Hydrogels for chronic wound healing, Adv. Mater. 33 (39) (2021).

[32] M. Anvarinejad, G. Pouladfar, A. Japoni, S. Bolandparvaz, Z. Satiary, P. Abbasi, J. Mardaneh, Isolation and antibiotic susceptibility of the microorganisms isolated from diabetic foot infections in Nemazee hospital, Southern Iran, J. Pathog. 2015 (2015) 328796.

[33] S. Regmi, S. Pathak, M.R. Nepal, P. Shrestha, J. Park, J.O. Kim, C.S. Yong, D. Choi, J. Chang, T.C. Jeong, G. Orive, S. Yook, J. Jeong, Inflammation-triggered local drug release ameliorates colitis by inhibiting dendritic cell migration and Th1/Th17 differentiation, J. Control. Release 316 (2019) 138–149.

[34] A. Rinaldi, R. Caraffi, M.V. Grazioli, N. Oddone, L. Giardino, G. Tosi, M.A. Vandelli, L. Calza, B. Ruozi, J.T. Duskey, Applications of the ROS-responsive Thioketal linker for the production of smart nanomedicines, Polymers-Basel 14 (4) (2022).

[35] B. Liu, S. Thayumanavan, Mechanistic investigation on oxidative degradation of ROS-responsive Thioacetal/Thioketal moieties and their implications, Cell Rep. Phys. Sci. 1 (12) (2020) 100271.

[36] N. Zheng, D. Xie, Z. Zhang, J. Kuang, Y. Zheng, Q. Wang, Y. Li, Thioketal-crosslinked: ROS-degradable polycations for enhanced in vitro and in vivo gene delivery with self-diminished cytotoxicity, J. Biomater. Appl. 34 (3) (2019) 326–338.

[37] X. Zhao, D. Pei, Y. Yang, K. Xu, J. Yu, Y. Zhang, Q. Zhang, G. He, Y. Zhang, A. Li, Y. Cheng, X. Chen, Green tea derivative driven smart hydrogels with desired functions for chronic diabetic wound treatment, Adv. Funct. Mater. 31 (18) (2021).

[38] Y. Huang, L. Mu, X. Zhao, Y. Han, B. Guo, Bacterial growth-induced tobramycin smart release self-healing hydrogel for Pseudomonas aeruginosa-infected burn wound healing, ACS Nano 16 (8) (2022) 13022–13036.

[39] J. Wang, J. Lin, L. Chen, L. Deng, W. Cui, Endogenous electric-field-coupled electrospun short Fiber via collecting wound exudation, Adv. Mater. 34 (9) (2022).

[40] H. Geng, P. Zhang, L. Liu, Y. Shangguan, X. Cheng, H. Liu, Y. Zhao, J. Hao, W. Li, J. Cui, Convergent architecting of multifunction-in-one hydrogels as wound dressings for surgical anti-infections, Mater. Today Chem. 25 (2022) 100968.

[41] C. Huang, L. Dong, B. Zhao, Y. Lu, S. Huang, Z. Yuan, G. Luo, Y. Xu, W. Qian, Anti-inflammatory hydrogel dressings and skin wound healing, Clin. Transl. Med. 12 (11) (2022) e1094.

[42] C. Tu, H. Lu, T. Zhou, W. Zhang, L. Deng, W. Cao, Z. Yang, Z. Wang, X. Wu, J. Ding, F. Xu, C. Gao, Promoting the healing of infected diabetic wound by an anti-bacterial and nano-enzyme-containing hydrogel with inflammation-suppressing, ROS-scavenging, oxygen and nitric oxide-generating properties, Biomaterials 286 (2022) 121597.

[43] L. Deng, C. Du, P. Song, T. Chen, S. Rui, D.G. Armstrong, W. Deng, The role of oxidative stress and antioxidants in diabetic wound healing, Oxidative Med. Cell. Longev. 2021 (2021).

[44] J. Yu, R. Zhang, B. Chen, X. Liu, Q. Jia, X. Wang, Z. Yang, P. Ning, Z. Wang, Y. Yang, Injectable reactive oxygen species-responsive hydrogel dressing with sustained nitric oxide release for bacterial ablation and wound healing, Adv. Funct. Mater. 32 (33) (2022).

[45] Y. Liang, J. He, B. Guo, Functional hydrogels as wound dressing to enhance wound healing, ACS Nano 15 (8) (2021) 12687–12722.

[46] M. Puthia, M. Butrym, J. Petrlova, A. Strömdahl, M.Å. Andersson, S. Kjellström, A. Schmidtchen, A dual-action peptide-containing hydrogel targets wound infection and inflammation, Sci. Transl. Med. 12 (524) (2020).
[47] H. Xia, Z. Dong, Q. Tang, R. Ding, Y. Bai, K. Zhou, L. Wu, L. Hao, Y. He, J. Yang, H. Mao, Z. Gu, Glycopeptide-based multifunctional hydrogels promote diabetic wound healing through pH regulation of microenvironment, Adv. Funct. Mater. 33 (29) (2023).
[48] H. Lu, C. Tu, T. Zhou, W. Zhang, Y. Zhan, J. Ding, X. Wu, Z. Yang, W. Cao, L. Deng, C. Gao, F. Xu, A ROS-scavenging hydrogel loaded with bacterial quorum sensing inhibitor hyperbranched poly-L-lysine promotes the wound scar-free healing of infected skin in vivo, Chem. Eng. J. 436 (2022) 135130.
[49] Z. Tu, M. Chen, M. Wang, Z. Shao, X. Jiang, K. Wang, Z. Yao, S. Yang, X. Zhang, W. Gao, C. Lin, B. Lei, C. Mao, Engineering bioactive M2 macrophage-polarized anti-inflammatory, antioxidant, and antibacterial scaffolds for rapid angiogenesis and diabetic wound repair, Adv. Funct. Mater. 31 (30) (2021).
[50] J. Li, Y. Hu, B. Hu, W. Wang, H. Xu, X. Hu, F. Ding, H. Li, K. Wang, X. Zhang, D. Guo, Lactose azocalixarene drug delivery system for the treatment of multidrug-resistant pseudomonas aeruginosa infected diabetic ulcer, Nat. Commun. 13 (1) (2022) 6279.
[51] Y. Xiong, Z. Lin, P. Bu, T. Yu, Y. Endo, W. Zhou, Y. Sun, F. Cao, G. Dai, Y. Hu, L. Lu, L. Chen, P. Cheng, K. Zha, M.A. Shahbazi, Q. Feng, B. Mi, G. Liu, A whole-course-repair system based on neurogenesis-angiogenesis crosstalk and macrophage reprogramming promotes diabetic wound healing, Adv. Mater. 35 (19) (2023) e2212300.
[52] B.M. Delavary, W.M. van der Veer, M. van Egmond, F.B. Niessen, R.H.J. Beelen, Macrophages in skin injury and repair, Immunobiology 216 (7) (2011) 753–762.
[53] M. Sharifiaghdam, E. Shaabani, R. Faridi-Majidi, S.C. De Smedt, K. Braeckmans, J. C. Fraire, Macrophages as a therapeutic target to promote diabetic wound healing, Mol. Ther. 30 (9) (2022) 2891–2908.
[54] D.G. Armstrong, A. Boulton, S.A. Bus, Diabetic foot ulcers and their recurrence, NEW ENGL. J. MED. 376 (24) (2017) 2367–2375.
[55] S.A. Eming, P. Martin, M. Tomic-Canic, Wound repair and regeneration: mechanisms, signaling, and translation, Sci. Transl. Med. 6 (265) (2014) 265sr6.
[56] Y. Li, J. Wang, D. Qian, L. Chen, X. Mo, L. Wang, Y. Wang, W. Cui, Electrospun fibrous sponge via short fiber for mimicking 3D ECM, J. Nanobiotechnol. 19 (1) (2021).
[57] P. Chen, K. Pan, N. Song, Y. Yang, C. Gu, P. Zhong, L. Li, M. Li, Y. Zhang, Z. Dai, L. Shangguan, C. Lei, Z. Liu, J. Zhang, R. Tang, C. Liu, S. Fan, X. Lin, A natural extracellular matrix hydrogel through selective nutrient restriction for hyperinflammatory starvation therapy, Matter-US 6 (2) (2023) 397–428.
[58] S. Cheng, X. Zhang, Q. Feng, J. Chen, L. Shen, P. Yu, L. Yang, D. Chen, H. Zhang, W. Sun, X. Chen, Astragaloside IV exerts angiogenesis and cardioprotection after myocardial infarction via regulating PTEN/PI3K/Akt signaling pathway, Life Sci. 227 (2019) 82–93.
[59] Y. Lu, Y. Wang, J. Zhang, X. Hu, Z. Yang, Y. Guo, Y. Wang, In-situ doping of a conductive hydrogel with low protein absorption and bacterial adhesion for electrical stimulation of chronic wounds, Acta Biomater. 89 (2019) 217–226.
[60] Z.A. Ali, A. Chakraborty, Y. Shamiya, S.P. Ravi, A. Paul, Leveraging the advancements in functional biomaterials and scaffold fabrication technologies for chronic wound healing applications, Mater. Horiz. 9 (7) (2022) 1850–1865.
[61] J.S. Chin, L. Madden, S.Y. Chew, D.L. Becker, Drug therapies and delivery mechanisms to treat perturbed skin wound healing, Adv. Drug Deliv. Rev. 149-150 (2019) 2–18.
[62] Y. Guan, H. Niu, Z. Liu, Y. Dang, J. Shen, M. Zayed, L. Ma, J. Guan, Sustained oxygenation accelerates diabetic wound healing by promoting epithelialization and angiogenesis and decreasing inflammation, Sci. Adv. 7 (35) (2021).